HHS Public Access

Author manuscript

J Mol Cell Cardiol Plus. Author manuscript; available in PMC 2024 July 02.

Published in final edited form as:

J Mol Cell Cardiol Plus. 2024 June ; 8: . doi:10.1016/j.jmccpl.2024.100075.

Roles of cMyBP-C phosphorylation on cardiac contractile dysfunction in *db/db* mice

Darshini A. Desai[a,1], **Akhil Baby**[a,b,1], **Kalyani Ananthamohan**[a], **Lisa C. Green**[a], **Mohammed Arif**[a], **Brittany C. Duncan**[a], **Mohit Kumar**[a,2], **Rohit R. Singh**[a,3], **Sheryl E. Koch**[a], **Sankar Natesan**[b], **Jack Rubinstein**[a], **Anil G. Jegga**[c,d], **Sakthivel Sadayappan**[a,*]

[a]Center for Cardiovascular Research, Department of Internal Medicine, Division of Cardiovascular Health and Disease, University of Cincinnati College of Medicine, Cincinnati, OH 45267, USA

[b]Department of Genetic Engineering, School of Biotechnology, Madurai Kamaraj University, Madurai 625021, India

[c]Division of Biomedical Informatics, Cincinnati Children's Hospital Medical Center, Cincinnati, OH, USA

[d]Department of Pediatrics, College of Medicine, University of Cincinnati, Cincinnati, OH, USA

Abstract

Type 2 diabetes mellitus (T2DM) is a metabolic disease and comorbidity associated with several conditions, including cardiac dysfunction leading to heart failure with preserved ejection fraction (HFpEF), in turn resulting in T2DM-induced cardiomyopathy (T2DM-CM). However, the molecular mechanisms underlying the development of T2DM-CM are poorly understood. It is hypothesized that molecular alterations in myopathic genes induced by diabetes promote the development of HFpEF, whereas cardiac myosin inhibitors can rescue the resultant T2DM-mediated cardiomyopathy. To test this hypothesis, a Leptin receptor-deficient *db/db* homozygous (Lepr *db/db*) mouse model was used to define the pathogenesis of T2DM-CM. Echocardiographic studies at 4 and 6 months revealed that Lepr db/db hearts started developing cardiac dysfunction by four months, and left ventricular hypertrophy with diastolic dysfunction was evident at 6

*Corresponding author at: Division of Cardiovascular Health and Disease, University of Cincinnati, 231 Albert Sabin Way, Cincinnati, OH 45267, USA. sadayasl@ucmail.uc.edu (S. Sadayappan).

[1]Equal contributions.

[2]Current address: Regeneron Pharmaceuticals Inc., Cardiovascular, Renal, and Fibrosis Research, Tarrytown, NY, USA.

[3]Current address: Amgen Research, Department of Cardiometabolic Disorders, Amgen, South San Francisco, California, USA.

Supplementary data to this article can be found online at https://doi.org/10.1016/j.jmccpl.2024.100075.

CRediT authorship contribution statement

Darshini A. Desai: Writing – review & editing, Writing – original draft, Validation, Resources, Project administration, Investigation, Formal analysis, Data curation, Conceptualization. **Akhil Baby:** Writing – review & editing, Writing – original draft, Validation, Data curation. **Kalyani Ananthamohan:** Writing – review & editing, Writing – original draft, Methodology, Formal analysis, Data curation. **Lisa C. Green:** Writing – review & editing, Writing – original draft, Validation. **Mohammed Arif:** Investigation, Data curation, Conceptualization. **Brittany C. Duncan:** Validation, Investigation, Data curation, Conceptualization. **Mohit Kumar:** Methodology, Investigation, Formal analysis, Data curation, Conceptualization. **Rohit R. Singh:** Writing – review & editing, Writing – original draft, Methodology, Investigation, Formal analysis, Data curation, Conceptualization. **Sheryl E. Koch:** Writing – review & editing, Writing – original draft, Formal analysis, Data curation. **Sankar Natesan:** Supervision. **Jack Rubinstein:** Supervision. **Anil G. Jegga:** Writing – original draft, Visualization, Supervision, Formal analysis. **Sakthivel Sadayappan:** Writing – review & editing, Writing – original draft, Supervision, Resources, Project administration, Funding acquisition, Conceptualization.

months. RNA-seq data analysis, followed by functional enrichment, revealed the differential regulation of genes related to cardiac dysfunction in Lepr *db/db* heart tissues. Strikingly, the level of cardiac myosin binding protein-C phosphorylation was significantly increased in Lepr *db/db* mouse hearts. Finally, using isolated skinned papillary muscles and freshly isolated cardiomyocytes, *CAMZYOS*® (mavacamten, MYK-461), a prescription heart medicine used for symptomatic obstructive hypertrophic cardiomyopathy treatment, was tested for its ability to rescue T2DM-CM. Compared with controls, MYK-461 significantly reduced force generation in papillary muscle fibers and cardiomyocyte contractility in the db/db group. This line of evidence shows that 1) T2DM-CM is associated with hyperphosphorylation of cardiac myosin binding protein-C and 2) MYK-461 significantly lessened disease progression *in vitro*, suggesting its promise as a treatment for HFpEF.

Keywords

cMyBP-C; Diabetes; HFpEF; *MYBPC3*; Mavacamten; Phosphorylation

1. Introduction

Heart failure (HF) is a leading cause of hospitalization affectin ~6.5 million Americans, and it is the costliest cardiovascular disorder in the United States [1,2]. More than half of heart failure patients are diagnosed with heart failure with preserved ejection fraction (HFpEF), a condition in which the heart has an intact capacity to eject but lacks the compliance to fill completely. HFpEF is often observed in the setting of left ventricular hypertrophy. However, it is, in essence, a complex heterogeneous disorder often associated with systemic comorbidities, including obesity, hypertension, diabetes, and aging, all associated with higher mortality [1,3]. Similar to heart failure with reduced ejection fraction (HFrEF) [4–7], which occurs when left ventricular ejection fraction (LVEF) ≤40 %, the survival rate of HFpEF patients over time remains poor, albeit for unclear reasons. HFpEF often involves impaired relaxation or increased stiffness of the left ventricle during diastole, the phase when the heart fills with blood. This results in decreased ventricular filling, leading to reduced stroke volume and cardiac output. The mechanisms underlying HFpEF are complex and multifactorial, and our understanding of them continues to evolve. One emerging area of interest is the role of myofilament dysfunction in the pathophysiology of HFpEF. Treatment modalities are limited to managing HFpEF by improving blood glucose levels and metabolism (Metformin, Sodium-glucose cotransporter 2 (SGLT-2) inhibitors, Glucagon-like peptide 1 (GLP-1) agonist, Dipeptidyl peptidase 4 (DPP4) inhibitors), blood pressure (Angiotensin-converting enzyme (ACE) inhibitors), heart rate (β-blockers), and volume/electrolyte status [8]. This underscores the importance of research aimed at identifying the molecular mechanisms governing HFpEF pathology and subsequently designing new targeted therapies to effectively manage this disease.

About 45 % of HFpEF patients have type 2 diabetes mellitus (T2DM) [9,10], markedly increasing the chances of hospitalization and risk of death [11–13]. T2DM patients show a greater incidence of diastolic dysfunction with pulmonary hypertension, lower exercise capacity, and higher long-term mortality rates [14]. Considering that approximately 30

and 84 million Americans have T2DM and prediabetes, respectively [15], the impact of T2DM comorbidity on HFpEF outcomes is striking. In general terms, HFpEF is exacerbated by T2DM secondary to diabetic cardiomyopathy (T2DM-CM). T2DM-CM is initially characterized by cardiac hypertrophy, increased left ventricular stiffness, wall thickness, myocardial fibrosis, dysfunctional remodeling, end-diastolic dimension, and reduced diastolic relaxation, as well as later systolic dysfunction, and, eventually, overt heart failure [16,17]. All these features are present in the absence of coronary artery disease or hypertension and without changing global cardiac pumping [18,19]. T2DM-related metabolic derangements, such as hyperglycemia, hyperinsulinemia, and lipotoxicity, favor the development of diastolic dysfunction and HFpEF [18,20]. This means that T2DM patients with even mild diastolic dysfunction face an increase in mortality after 5 years by >8-fold [21]. Importantly, diastolic dysfunction is now being recognized in obese youth with T2DM. Therefore, given the epidemic of obesity associated with T2DM, diabetic juveniles are at risk for early HFpEF phenotype [22–26], but with limited treatment options [27]. One promising treatment option for adults with diabetic cardiomyopathy is the use of SGLT2 inhibitors. Previous studies have shown that SGLT2 inhibitors help in improving the energetics [28], metabolism and diastolic function [29], reducing renal deterioration [30], and oxidative stress/inflammation [31]. Several recent clinical trials have demonstrated that treatment with an SGLT2 inhibitor significantly decreases cardiac events and hospitalization [32–36]. Interestingly, however, these treatments show limited efficacy in patients with ejection fractions >65 [37]. This calls for renewed efforts to improve upon current treatments to prevent HFpEF and subsequent progression to HFrEF.

Myosin binding protein-C (MyBP-C) is a trans filament contractile and thick filament accessory protein in striated muscles. The cardiac paralog, cMyBP-C, plays an important role in regulating contraction in the heart [38]. cMyBP-C comprises eleven domains with seven immunoglobulin-like and three fibronectin type III-like domains, numbered C0–C10 from the N-terminus, and a regulatory phosphorylation M-domain between C1 and C2 [39]. The M-domain in cMyBP-C plays a critical functional role in binding to both actin and myosin to modulate actomyosin interactions, rate, and force of contraction [40]. M-domain has three phosphorylation sites, serine 273, 282, and 302, which regulate contractility in the heart [41–43]. Phosphorylation of cMyBP-C at these serine sites is mediated by various protein kinases like PKA, PKC, PKD, p90 S6, and CaMKII [44–47]. When any one of these kinases phosphorylates cMyBP-C in response to various pathophysiological conditions, it removes a brake, accelerating the rate of actomyosin interactions and leading to enhanced cardiac contractility referred to as hypercontractility [48,49]. Specifically, cMyBP-C phosphorylation influences the Mg^{2+}-ATPase activity of myosin, the kinetics of cross-bridge cycling, and the rate of relaxation [46,47,50,51]. It is well known that phosphorylation levels increase during the early development of cardiac hypertrophy [41], but whether this is an early sign of diastolic dysfunction in T2DM-CM is unknown.

As previously suggested [11–13], diastolic dysfunction in T2DM patients is characterized by the proximate etiologic factors of increased energy demand, calcium transients, and cardiomyocyte stiffness, leading to concentric cardiac hypertrophy. Beyond this, however, the molecular mechanism(s) underlying such diastolic dysfunction in T2DM remain(s) to be elucidated. Meanwhile, interventions, such as blood pressure control, heart rate control,

and diuretics, have focused on improving the clinical parameters, whereas treating diastolic dysfunction is still challenging [8,52]. Therefore, the present paper examined the etiology of T2DM-CM, the possible association of cMyBP-C hyperphosphorylation in its pathogenesis, and whether the myosin inhibitor Mavacamten (MYK-461) [53] has an impact on improving the contractile properties of cardiomyocytes of diabetic mice. Such systematic investigation aims to elucidate the molecular basis of the T2DM-CM associated with diastolic dysfunction and potential therapeutic targets. To accomplish this, a Leptin receptor-deficient (*db/db*) mouse model was employed since it has been previously reported as a model to study the mechanism of the human T2DM-CM [54,55] and diastolic dysfunction [56]. These animals exhibit an autosomal recessive mutation in the leptin receptor gene and features typical of T2DM, including hyperphagia, obesity, and hyperglycemia [57]. Moreover, *db/db* mice can exhibit different types of cardiac remodeling, including diastolic dysfunction [56,58]. Our results show that *db/db* mice undergo cardiac remodeling starting from 4 months and progressing to cardiac hypertrophy at six months. Interestingly, *db/db* mouse hearts show hyperphosphorylated cMyBP-C at serine 273 and 302 compared to their wild-type (WT) controls. In addition, the impaired contractility and increased force generation observed in skinned papillary muscles and isolated cardiomyocytes of *db/db* mice were attenuated by MYK-461. Therefore, our study supports the administration of MYK-461 as a potential candidate for treating T2DM-mediated CM and HFpEF.

2. Methods

2.1. Mouse models

Male and female C57BL/K6sJ-Lepr db/Lepr db diabetic (*db/db*) mice and nondiabetic C57BL/WT mice were obtained from Jackson Laboratories (Bar Harbor, ME) and used for experiments in this work from 2 months of age. Mice were housed in an animal facility with controlled ambient temperature at 20 °C, humidity at 60 %, and 12 h of light/dark cycles. Mice were fed *ad libitum* with a standard diet. Mice were sacrificed by anoxia with CO_2 inhalation, followed by cervical dislocation, in accordance with the American Veterinary Medical Association Guidelines on Euthanasia (2020 Edition). All experiments were performed on animals with age- and sex-matched controls at four and six months of age. The University of Cincinnati IACUC approved all experiments using animals, as detailed in this work, and the policies and practices recommended in the NIH Guide for the Use and Care of Laboratory Animals were strictly followed.

2.2. Blood glucose and insulin levels

For measurements of blood glucose and insulin, all mice from both groups were fasted for 16 h prior to sampling. Feed was taken from cages at 6 pm in the evening until 10 am the next morning. Blood was collected after 16 h of fasting by making a small incision in the tail vein of the mice. Blood sugar was measured using a glucometer (Contour Next, Blood Glucose Monitoring System; Catalog no. 816685237379), whereas 100 μL of blood was drawn to measure plasma insulin levels using the Mouse Ins1 / Insulin-1 ELISA Kit (Sigma Aldrich: catalog no. RAB0817) according to the manufacturer's directions.

2.3. Echocardiography

Echocardiographic studies were performed to measure cardiac function as described previously [59–61]. Briefly, 4- or 6-month-old WT and *db/db* mice were anesthetized with 2.5 % isoflurane and placed on the heated stage of a Vevo 2100 (VisualSonics, Toronto, Canada) echocardiography machine. Using the MS400 probe (30mHz), parasternal long axis (PSLAX) and short axis (SAX) images were recorded, as well as analyzed on a separate workstation, using the Vevo Strain software (Vevo 2100, v5.7.1, VisualSonics, Toronto, Canada). Ejection fraction (EF), fractional shortening (FS), left ventricular systolic diameter and volume (LV dia;s and LV vol;s), left ventricular posterior wall end diastole and end systole (LVPW:d and LVPW;s), interventricular septal end diastole and end systole (IVS;d and IVS;s), and LV mass were all obtained from SAX M-mode images using Vevo software [61]. Diastolic function was evaluated using pulsed wave and Tissue Doppler. From an apical long-axis view, transmitral inflow velocities were recorded by setting the spike in the mitral orifice close to the tip of the mitral leaflets. Peak early- and late-diastolic transmitral velocities (E and A waves) were measured from pulsed wave Doppler spectral waveforms. E′ (early diastolic myocardial relaxation velocity) was measured from tissue Doppler spectral waveforms, and E/E′ ratio was calculated [59]. WT and *db/db* mice were assessed on the same day by the same technician in a blinded manner to minimize variation in the recordings and analysis. For echocardiography measurements, 8 WT mice (5 females and 3 males) and 9 *db/db* mice (5 females and 4 males) were used.

2.4. Protein expression and quantification

Total proteins were extracted from the whole hearts of 6-month-old mice. Hearts were snap-frozen, homogenized in ice-cold PSB lysis buffer (Biorad #1632145) with protease and phosphatase inhibitors (Thermo Scientific #78442), and sampled for protein concentration by the Bradford assay (Thermo Scientific #23226). 30 μg of protein samples from lysates were run on an SDS-PAGE using 4–20 % polyacrylamide gels using Precision Plus Protein™ All Blue prestained protein molecular weight standard ladder (Bio-Rad, catalog no. 1610373; 10–250 kDa). Next, the gel was transferred to 0.2-μm nitrocellulose membranes using Bio-Rad transfer buffers. Nitrocellulose membranes were then incubated in a blocking buffer with 5 % *w/v* nonfat dry milk for at least 1 h at room temperature. Afterward, immunoblot membranes were incubated with the respective primary antibodies diluted in buffer with 5 % w/v nonfat dry milk and probed overnight at 4 °C. The following commercial primary antibodies were used: cTnI (Abcam, #ab47003), phosphoserine 22/23 cTnI (Invitrogen, #PA5–38341), monoclonal anti-cMyBP-C antibody to recognize total protein (Santa Cruz Biotechnology, #sc-137237), and anti-cMyBP-C phosphoserine 273, 282, and 302 antibodies [48]. Anti-GAPDH antibody was used as a loading control (Fitzgerald, catalog no. 10R-G109a). The fluorescent mouse- or rabbit-specific secondary antibodies used were bought commercially (1:5000, LI-COR Biosciences), diluted in buffer with 5 % *w/v* nonfat dry milk, and incubated for 1 h at room temperature with gentle shaking. Nitrocellu-lose membranes were then washed with TBS buffer for five times, and the membranes were then imaged using the Odyssey FC imaging system (LI-COR Biosciences). Total protein and phosphorylation levels of cMyBP-C and cTnI proteins were detected by dual-color Western blotting using two IR fluorophores. All Western blots with their protein bands were quantified using Fiji software(NIH). Phosphorylated cTnI

was expressed as pSer22–23/cTnI and cTnI/GAPDH, and phosphorylated cMyBP-C was expressed as normalized to total cMyBP-C (pSer302/cMyBP-C, pSer282/cMyBP-C, and pSer273/cMyBP-C) and total cMyBP-C normalized to GAPDH (total cMyBP-C/GAPDH) [40,62,63].

2.5. RNA sequencing

Mice hearts were dissected at 6 months of age, followed by total RNA isolation using an RNA isolation kit (Qiagen, cat# 763134), according to the manufacturer's instructions. Total RNA concentration and quality (A260/280 ratio≥2.0) were evaluated using a Nanodrop spectrophotometer (ThermoFisher Scientific). The quality of total RNA was further measured using the Agilent 2100 Bioanalyzer (Agilent, Santa Clara, CA) and sequenced using *DNBSEQ*™ sequencing *technology* (BGI Global Genomic Services, Cambridge, MA, USA). In brief, the polyadenylation (polyA) enriched mRNAs were purified using poly-T oligo-attached magnetic beads. Following purification, the mRNA was fragmented and copied into first-strand cDNA using reverse transcriptase and random primers. This was followed by second-strand cDNA synthesis and adaptor ligation. The products were then purified and enriched by PCR amplification, quantified by Qubit, and heat-separated to form single-stranded circular DNA (circDNA). DNA nanoballs (DNBs) were generated with circDNA by rolling-circle replication (RCR) to increase the fluorescence signal during sequencing. DNBs were loaded into the patterned nanoarrays using the high-intensity DNA nanochip technique and sequenced through combinational Probe-Anchor Synthesis.

The sequencing data reads mapped to rRNAs were removed, followed by filtering of reads to remove reads with adaptors, unknown bases, and low-quality reads. Then, the reads were mapped to the *Mus musculus* reference genome, version GCF_000001635.26_GRCm38.p6 (NCBI), using Bowtie2 [64] and HISAT2. The gene expression level was calculated using the RSEM [65] software package to estimate gene expression levels from RNA-Seq data. Finally, DEGs (differentially expressed genes) between samples were identified using DESeq2. DESeq2 is based on negative binomial distribution and was performed according to Michael I, et al. [66] (DEseq2 Parameters: Log_2Fold Change ≥2.00 and Adjusted *P*-value ≤0.05). For this exploratory work, we selected the top up-and downregulated genes using a fold change cutoff value of 1.5 (Log_2Fold Change Cutoff 0.5849, Adjusted P-value ≤ 0.05). The RNA sequencing data have been deposited in NCBI's Gene Expression Omnibus and are accessible through GEO series accession number GSE235934. Functional enrichment analysis of differentially expressed gene sets was conducted using the ToppFun application of the ToppGene Suite [67]. Cytoscape was used to represent the network of select significantly enriched biological processes and pathways [67].

2.6. pCa-force measurements

Papillary fibers were dissected from the left ventricles of 6-month-old C57/BL6 WT and *db/db* mice, as described previously [40]. Dissection and permeabilization (skinning) of papillary fibers were performed as described previously [43]. Papillary fibers were incubated overnight for skinning in 1 % Triton X-100 containing relaxing buffer prepared with 55.74 mmol/L potassium propionate, 5.5 mmol/L magnesium chloride, 7 mmol/L ethylene glycol bis(2-aminoethyl)tetraacetic acid, 5 mmol/L dithiothreitol, 0.02 mmol/L calcium

chloride, 15 mmol/L creatine phosphate, 100 mmol/L *N,N*-bis(2-hydroxyethyl)-2-amino ethane sulfonic acid, and 4.7 mmol/L adenosine triphosphate. The pH was adjusted to 7.0 with 4 mol/L potassium hydroxide, and ionic strength was maintained at 180 with potassium propionate at pCa 9.0 and temperature at 4 °C. Papillary muscle was cut into fiber bundles approximately 1 mm in length. Straight and uniform bundles were then selected and attached with aluminum t-clips at both ends. Fibers were next washed with the fresh relaxing solution. Finally, the t-clipped fiber bundles were connected to a length controller on one side and a force transducer on the other side of the t-clip (both from Aurora Scientific, Inc.). Sarcomere length was set at 2.0 μm and monitored with Aurora's HVSL system. The area and length of muscle were measured using a microscope with a built-in micrometer (Aurora Scientific, Inc., resolution, ~10 μm), and those dimensions were used to normalize the force and sarcomere length of each fiber. The attached fiber bundles were tested for strength and rundown by exposure to the maximum calcium-activating solution at the start and end of the experiment. The isometric force of a skinned papillary fiber was measured as a function of calcium concentration. The fiber was exposed to increasing calcium solutions at pCa 6.3, 6.0, 5.8, 5.7, 5.6, 5.4, and 4.5 with or without MYK-461. Fibers were incubated for 5 min with MYK-461 (2 μM) or vehicle in all groups before measurements. The vehicle was DMSO and was measured as a control. The chemical makeup of the maximal calcium solution (pCa 4.5) was similar to that of the relaxing buffer, but containing 7 mmol/L calcium chloride. Force measurements were also normalized to a cross-sectional area and corrected for the rundown [68]. Fibers exceeding the 20 % rundown were excluded from further data analysis. All data were acquired using Aurora's 600 A Real-Time Muscle Data Acquisition and Analysis System. Each force-calcium relationship was fitted to a modified Hill equation (Force/Forcemax = [Ca2+]n/(pCa_{50}n + [Ca^{2+}]n), where n is the Hill slope. The Hill equation is a mathematical model describing the relationship between the concentration of calcium and the force produced in the muscle. The pCa_{50} value was also determined by fitting the force-calcium relationship to a Hill equation. The pCa_{50} corresponds to the concentration of calcium at which half of the maximal force is produced. The rate of force (tension) redevelopment (k_{tr}) was measured (Aurora Scientific, Inc.), as previously described [43]. At submaximal pCa of 5.7, when the fiber reached steady-state force for 20 milliseconds, it was shortened by 20 % before rapidly (~1 millisecond) stretching back to its original length. After fitting this slack-stretch treatment against the time required to a one-phase association curve, k_{tr} was calculated by fitting the force redeveloped in the skinned papillary muscle fiber.

2.7. Contractility measurements in isolated adult ventricular cardiomyocytes

Cardiomyocyte contractility and Ca^{2+} transients were measured simultaneously at room temperature, as described previously [48,69]. Briefly, mouse hearts from 6-month-old WT and db/db mice were excised after administering anesthesia (Euthasol, 200 mg/kg IP, Virbac AH, Inc., Texas), mounted in a Langendorff perfusion apparatus, and perfused with Ca-free Tyrode's solution at 37 °C for 3 min. Tyrode's solution consisted of 140 mM NaCl, 4 mM KCl, 1 mM $MgCl_2$, 10 mM glucose, and 5 mM HEPES, pH 7.4. Perfusion was then switched to the same solution containing Liberase (0.25 mg/ml, Roche) until the heart became flaccid (~8–10 min). Isolated cardiomyocytes were incubated at room temperature for 15 min in the media containing Ca^{2+}-sensitive Fura-2 dye at a final concentration of

1.0 μM (Invitrogen) and subsequently washed with Tyrode's solution twice for 10 min. After that, live cells were placed in a perfusion chamber on the stage of an inverted Nikon eclipse TE2000-U fluorescence microscope. Using a video-based sarcomere length detection system (IonOptix, Milton, MA, USA), sarcomere shortening was measured. To quantify the intracellular Ca^{2+} transients, Fura-2 dye was excited at 340 and 380 nm and acquired at an emission wavelength of 515 ± 10 nm using a spectrofluorometer (IonOptix) restricted to a single cell. Simultaneous measurements of sarcomere mechanics and Ca^{2+} kinetics in isolated cardiomyocytes were also performed in the presence of 250 nmol/l of MYK-461 or vehicle alone (control). MYK-461 was purchased from *MedChemExpress* (MCE, catalog no. HY-109037), dissolved in DMSO, and diluted in Tyrode's solution to achieve a final concentration of 250 nM MYK-461 at room temperature, as described earlier. The data were analyzed by IonOptix LLC analytic software [70].

2.8. Statistical analysis

Data were expressed as mean ± S.E.M or S·D and were obtained using GraphPad Prism 9.3. For cardiomyocyte contractility measurements, 8–12 cardiomyocytes were analyzed for each heart with each heart represented as a single n ($n = 3$ hearts). For multiple-group comparisons, one-way ANOVA and two-way ANOVA were performed, followed by Tukey's multiple-comparison test with single pooled variance or Sidak's Multiple comparison test. All protein band intensities were quantified using Fiji software (NIH). Densitometric values from each protein were normalized with the loading control, GAPDH. Phosphorylation levels were further normalized with their total specific proteins. WT control values were converted to a value of 1, and the values of other groups were normalized and expressed as a fold change relative to the WT. Protein expression and phosphorylation levels were quantitatively compared using an unpaired *t*-test. A repeated-measurements two-way ANOVA test was performed, followed by Tukey's multiple-comparison test to analyze drug efficacy, before and after administration, on multiple groups. Data values with $p \leq 0.05$ were deemed significant.

3. Results

3.1. Lepr db/db mice exhibited a diabetic phenotype and obesity

Lepr *db/db* mice were assessed for developing T2DM at an early stage (Supplemental Fig. 1A). The *db/db* mice were visibly obese at six months of age, as evidenced by their increased body weight (BW) (Supplemental Fig. 1B). Heart weight (HW) was significantly elevated in *db/db* mice compared to WT mice (Supplemental Fig. 1C). The HW/BW ratio of *db/db* mice was significantly lower than that of WT controls (Supplemental Fig. 1D), which could be explained by the much higher BW of *db/db* mice. However, HW/Tibial length (TL) ratios (Supplemental Fig. 1E–F) were significantly elevated in *db/db* compared to WT mice at six months of age, demonstrating the presence of cardiac hypertrophy.

To evaluate the development of T2DM in *db/db* mice, blood glucose and plasma insulin levels were also measured at various time points (2, 4, and 6 months). As expected, db/db mice showed higher glucose levels than WT mice at all time points (Supplemental Fig. 1G). Interestingly, blood glucose levels were reduced at the age of 4 months and 6 months

compared to 2 months of age in *db/db* mice. Plasma insulin levels were significantly higher in *db/db* mice, starting at 4 months and persisting until 6 months of age, compared to WT mice, indicating hyperinsulinemia, which is a diagnostic feature of T2DM (Supplemental Fig. 1H). Overall, these data confirmed the development of diabetic features and obesity in Lepr *db/db* mice, resulting in the development of cardiac hypertrophy.

3.2. Cardiac function of diabetic Lepr db/db mice is consistent with the development of HFpEF

Previous studies have shown that Lepr *db/db* mice exhibit cardiac remodeling manifested as either systolic or diastolic dysfunction [71]; therefore, we performed echocardiographic analysis on these mice for signs of cardiac hypertrophy (Supplemental Fig. 1). Our echocardiographic analysis and measurements (Fig. 1A, Table 1) revealed hyper-dynamic systolic function in *db/db* mice from 4 to 6 months of age, whereas WT mice exhibited systolic function at levels usually considered “low normal” (Fig. 1B & C). This finding is consistent with increased LV mass, IVS;s, IVS;d, LVPW;s, and LVPW;d noted at 6 months (Fig. 1D–H), indicating the development of LV hypertrophy in *db/db* mice compared to WT mice. Simultaneously, significantly lower E/A and E/E′ ratios (mitral inflow parameter) were also noted in *db/db* mice at 6 months of age, indicating diastolic dysfunction (Fig. 1I & J). Taken together, these findings are suggestive of T2DM-CM, or cardiac hypertrophy, as an underlying cause for diastolic dysfunction, and are consistent with the HFpEF phenotype.

3.3. Pathogenic dysregulation of cardiac genes in Lepr db/db mice

At six months of age, *db/db* mice exhibited cardiac hypertrophy (Supplemental Fig. 1) and HFpEF phenotype (Fig. 1). Accordingly, RNA sequencing was performed to identify the molecular regulators of altered cardiac function in *db/db* mice. Bioinformatics data analysis revealed several differentially regulated genes (DEGs) in *db/db* mice compared to WT mice (Fig. 2A). A total of 150 genes were significantly upregulated, while 57 genes were downregulated in *db/db* mice hearts (Adjusted *P*-Value<0.05 and Fold Change Cutoff 1.5) (Fig. 2B–C, Supplemental File 1). Enrichment analysis revealed that most upregulated genes were associated with clinical phenotypes of cardiac disease, such as cardiomyopathy (primary and familial), cardiac hypertrophy, congestive heart failure, heart decompensation, and myocardial ischemia.

Gene ontology (GO) pathway analysis for these DEGs revealed that diabetic- and obesity-related molecular pathways were all dysregulated. These included apoptosis, inflammation, hypoxia, circadian rhythm, apelin signaling, adipogenesis, p53 signaling, p38 MAPK cascade, and cellular responses to insulin, lipid, and glucocorticoid. Similarly, cardiac muscle cell contraction and regulation of arterial blood pressure-related genes were also deregulated (Fig. 2D, Supplemental File 1). Notable upregulated genes were those related to cytoskeletal and sarcomeric structure, including TroponinT2 (*Tnnt2*) and Syntrophinα1 (*Snta1*); muscle cell proliferation and development gene Myostatin (*Mstn*); *KCNA5* (Potassium Voltage-Gated Channel Subfamily A Member 5), protein-coding gene associated with Atrial Fibrillation, Angiotensinogen (*Agt*) and (*Kcnk1*); and cardiac morphogenesis gene *HAND2* (heart and neural crest derivatives expressed 2).

Similarly, genes associated with apoptosis, including DNA-damage-inducible transcript 4 (*Ddit4*) and Fas cell surface death receptor (*Fas*); inflammatory genes like CCAAT/enhancer-binding protein delta (*Cebpd*) and Nfκb Inhibitor-α (*Nfkb-iα);* and mitochondrial membrane-associated proteins Bcl2-like1 (*Bcl2l1*) and Uncoupling protein 2 (*Ucp2*), also displayed a significant increase in expression. On the other hand, Apelin (*Apln*), Apelin receptor (*Aplnr),* Natriuretic peptide B (*Nppb*), and Unc-45 myosin chaperone B (*Unc45b*) were significantly downregulated in *db/db* mouse hearts. Collectively, these data suggest that the dysregulation of key cardiac genes in *db/db* mice most likely contributes to the induction of pathologic cardiac remodeling which, in turn, leads to T2DM-CM.

3.4. cMyBP-C hyperphosphorylation is an early sign of HFpEF and diastolic dysfunction in T2DM-CM

We have demonstrated that *db/db* mice display cardiac hypertrophy and diastolic dysfunction phenotype with dysregulation of genes involved in cardiac muscle function (Figs. 1–2, Supplemental Fig. 1 and Supplemental File 1). Next, we asked if the contractile function of cardiac muscle is affected in *db/db* mice. The phosphorylation status of the cMyBP-C isoform is crucial for regulating cardiac contractility. Therefore, three phosphorylation sites of cMyBP-C at serine 273, 282, and 302 were next investigated for their role in regulating the availability of myosin heads interacting with actin and, hence, playing a critical role in cardiac function [41–43]. Normal phosphorylation of cMyBP-C occurs under basal conditions, whereas dephosphorylation of cMyBP-C is associated with such well-documented pathological consequences as heart failure. Here, we are concerned with the effects of hyperphosphorylation of cMyBP-C, which is associated with accelerated cardiac contractility [72]. It is well established that hyperphosphorylation of cardiac troponin I, which has several phosphorylation sites, can accelerate cardiac contractility [73]. Based on these reports, we asked if the expression and phosphorylation levels of cMyBP-C and cardiac troponin I (cTnI) might play an integral role in triggering T2DM-CM. Specifically, we focused on the potential pathological consequences of hyperphosphorylation of cMyBP-C. To make this assessment, basal phosphorylation levels of cMyBP-C at Ser-273, Ser-282 and Ser-302 were measured in *db/db* and WT mice at 6 months of age using Western immunoblotting of the cardiac proteome (Fig. 3A). Strikingly, basal phosphorylation levels of cMyBP-C at Ser-273 and Ser-302, which are targeted by PKC [41], were significantly increased in *db/db* mice hearts compared with WT hearts (Fig. 3B–E). However, the phosphorylation site at Ser-282, also a target of PKA [41], was unaffected. Similarly, the phosphorylation of cTnI at Ser 22/23, another target of PKA, was unaltered in *db/db* mice hearts (Fig. 3F–G). These are signs indicating that PKC-mediated increase in cMyBP-C phosphorylation at Ser-273 and Ser-302 could play a role in the pathogenesis of T2DM-CM in Lepr *db/db* hearts.

3.5. MYK-461 rescues altered contractile parameters in Lepr db/db mice

The hyperphosphorylation of cMyBP-C protein accelerates cardiac contractility [41–43,72], but the effect of MYK-461 on contractile function is deceleration. Since we observed elevated phosphorylation of cMyBP-C mediated by PKC (Fig. 3), we next investigated the contractile properties of *db/db* mice heart muscles. We measured the contractile parameters in skinned papillary muscle fibers of age-matched Lepr *db/db* and WT mice with and

without treatment with MYK-461, a myosin inhibitor, that serves to reduce the interaction between actin and myosin [74]. Maximal force (F_{max}) produced per cross-sectional area with increasing calcium concentration, calcium sensitivity (pCa_{50}), and rate of force redevelopment (k_{tr}) were compared across both groups (Fig. 4A, Table 2). Skinned papillary muscle from *db/db* mice treated with vehicle displayed significantly elevated contractile features compared with those of WT mice (Fig. 4B–C). The mean maximal force produced at the maximal calcium concentration of pC_a 4.5 was 42.1 ± 4.72 mN/mm^2 for *db/db* mice compared to 31.9 ± 2.75 mN/mm^2 for WT mice (Fig. 4B–C, $p < 0.001$). Similarly, means of pCa_{50} (Fig. 4D–E) and k_{tr} (Fig. 4F–G) were significantly higher in the db/db mice (5.68 ± 0.03 s^{-1} and 8.84 ± 2.02 s^{-1}, respectively) as opposed to WT mice (5.61 ± 0.02 s^{-1} and 5.25 ± 1 s^{-1}, respectively) ($p < 0.001$). However, when the skinned papillary fibers of Lepr db/db mice were treated with 2 μM of MYK-461, all elevated contractile parameters reverted to basal levels, as observed in WT mice. Indeed, MYK-461 treatment was found to lower mean F_{max}, $pCa_{50,}$ and k_{tr} values (33.8 ± 3.14 mN/mm^2, 5.61 ± 0.02 s^{-1} and 4.332 ± 1.55 s^{-1}, respectively) in *db/db*, values comparable to those of WT mice ($p \leq 0.05$). These results show the efficacy of MYK-461 in the potential rescue of altered contractile parameters seen in cardiac muscles of db/db mice with HFpEF [58].

3.6. MYK-461 alleviates contractile dysfunction in cardiomyocytes of Lepr db/db mice without affecting calcium handling

Our experiments with skinned papillary muscles suggest changes in contractile parameters of *db/db* myofibril level (Fig. 4), a phenomenon that inspired us to further study the contractile properties and calcium dynamics at individual myocyte level using cardiomyocytes isolated from whole hearts of *db/db* and WT mice at six months of age, using the IonOptix system (Fig. 5A, Table 3). Isolated cardiomyocytes from *db/db* mice treated with vehicle showed an increase in the amplitude of basal cell contraction or fractional shortening (11.43 ± 0.55 %) compared to cardiomyocytes from WT mice hearts (7.26 ± 0.41 %) (Fig. 5B). Similarly, the rate of sarcomere contraction (contraction velocity) was elevated in db/db cardiomyocytes (2.53 ± 0.19 μm/s) compared to WT cardiomyocytes (1.78 ± 0.08 μm/s) at baseline (Fig. 5C). However, upon treatment (250 nM) with MYK-461, fractional shortening was significantly decreased in *db/db* cardiomyocytes (8.67 ± 0.54 %) compared to WT cardiomyocytes (Fig. 5B). Furthermore, contraction velocity (2 ± 0.12 μm/s) also improved in *db/db* cardiomyocytes upon MYK-461 treatment (Fig. 5C). To avoid saturating single cardiomyocytes with the drug, a lower dose of MYK-461 was used for contractile and calcium measurements.

However, even though diastolic relaxation was slower in *db/db* cardiomyocytes (0.48 ± 0.02 s) than in WT cardiomyocytes (0.3 ± 0.01 s), MYK-461 treatment did not improve this parameter (Fig. 5D). We also examined calcium handling properties in *db/db* cardiomyocytes by measuring the amplitude and kinetics of intracellular calcium-transients in isolated cardiomyocytes from *db/db* and WT hearts. Results show no difference in the time constant for calcium decay (tau) between *db/db* cardiomyocytes (0.27 ± 0.01 s) and WT cardiomyocytes (0.26 ± 0.01 s) (Fig. 5E). Nor do results show any change in Ca^{2+} transient amplitude, as indicated by Fura-2 ratio (340/380 nm) between *db/db* cardiomyocytes (0.20 ± 0.01 nm) and WT cardiomyocytes (0.19 ± 0.01 nm) at baseline or

with MYK-461 treatment (Fig. 5F). This calcium dataset suggests that MYK-461 does not interact with, or affect, calcium handling in cardiomyocytes, but rather improves contractile dysfunction in *db/db* cardiomyocytes.

4. Discussion

Diabetes is projected to be the seventh leading cause of death by 2030 [75], likely owing to progressive left ventricular diastolic dysfunction [76], HFpEF, and ultimately frank Dilated cardiomyopathy (DCM) [18,77–79]. Based on an obesity-related increase in T2DM, HFpEF is now the most common type of heart failure [80–84] and is associated with sudden cardiac death (SCD). Since no effective treatments for HFpEF are available [1,8], it accounts for ~300,000 deaths annually in the United States [85]. As stressed earlier, the presence of both HFpEF and T2DM is associated with increased morbidity and mortality [1,86–88]. HFpEF in the setting of T2DM and DCM is directly linked to classic T2DM metabolic abnormalities, including hyperglycemia, lipotoxicity, and hyperinsulinemia with left ventricular hypertrophy and diastolic left ventricular dysfunction [18]. Decreased diastolic filling (preload) is a hallmark of impaired relaxation, significantly decreasing stroke volume. In apparent compensation, cardiomyocytes of patients with HFpEF are primarily associated with increased collagen content at the cellular level. At the organ level, patients present with cardiac hypertrophy at a later stage in the development of T2DM. Despite such abnormalities in the myocardium and multiple impacts thereof, including the inability of *mitochondrial membrane potential* ($\Delta\Psi m$) to meet the energy demands needed to counter such maladaptive changes, no therapy has been developed to target cardiac muscle and directly treat HFpEF. Similarly, while elevated circulating glucose and free fatty acids promote a series of consequences of diverse metabolic effects in cardiomyocytes, translating this knowledge into an effective intervention remains to be accomplished.

In this study, Lepr *db/db* mice developed diabetic phenotypes marked by elevated blood glucose and plasma insulin levels within the first few months of life (Supplemental Fig. 1). These mice showed marked obesity compared to their WT counterparts at 6 months of age, and, importantly, they also exhibited cardiac hypertrophy (Supplemental Fig. 1) [56,89–91]. Similar results were experimentally reproduced *via* echocardiographic analysis of *db/db* and WT mice at 4 and 6 months of age, and the impairment of cardiac functions and HFpEF phenotype was confirmed (Fig. 1). Thus, the *db/db* mouse was an excellent model for studying T2DM-CM and testing potential treatments. RNA sequencing comparing cardiac gene expression in *db/db versus* WT revealed significant dysregulation of several biological processes related to obesity, diabetes, and cardiac function (Fig. 2).

The key molecular mechanisms of pathological cardiac hypertrophy are included as key features in the etiology of HFpEF [92]. Accordingly, we observed a functional enrichment of gene sets involved in the p38 MAPK pathway, cardiac muscle contraction, and the voltage-gated potassium channel complex. Consistent with previous reports of the hypertrophic stage of heart failure, we observed upregulation of the circadian gene *Ciart1* [93]. Among the upregulated genes with the highest fold change difference (log FC > 2), *Mstn*, which provides instructions for the protein myostatin, has been previously reported as a metabolic biomarker, and its elevated levels in circulation were associated with heart failure; however,

its role in HFpEF has yet to be explored [94–96]. Finally, despite our surprise upon observing a downregulation in the levels of cardiac NPPB, a member of the natriuretic peptide family that encodes a secreted protein that functions as a cardiac hormone, a few studies have reported that the levels of NPPB in heart failure are low and that the proportion of patients with low NPPB is higher in the HFpEF group compared to HFrEF [97–99]. This calls for additional studies and supporting data to validate low NPPB levels as a prognosis for HFpEF in diabetes. In sum, while the role of cardiac metabolism in HFpEF is only partially explained, microvascular dysfunction might be a possible reason for the hypoxic condition in HFpEF hearts [100], thus justifying Hifα upregulation and the observed enrichment of DEGs involved in the regulation of vasculature development (Supplemental File 1).

In this study, we next investigated the effects of T2DM on the expression and phosphorylation of the crucial sarcomere regulatory protein cMyBP-C and the contractile function of *db/db* heart at both myofibril and myocyte levels. For the cMyBP-C, regulatory phosphorylation *in vivo* by PKA upon adrenergic stimulation is linked to the modulation of cardiac contraction [50]. Human and mouse cMyBP-C has three phosphorylation sites per molecule [101], which the skeletal isoform lacks. Previous studies from our lab and others have demonstrated the importance of cMyBP-C expression and phosphorylation in the context of cardiac physiology and dysfunction [45,102]. cMyBP-C is a thick filament-associated protein that regulates myosin-actin interactions necessary for cardiac contraction [43]. Three critical phosphorylation sites exist in the myosin-interacting domain of cMyBP-C: serines 273, 282, and 302. This region of the N-terminus binds to the S2 segment of myosin [103–107], close to the lever arm domain. When these sites are phosphorylated, cMyBP-C exhibits less binding to myosin, freeing the myosin heads to interact with actin and increasing cardiomyocyte contraction. Conversely, a decrease in phosphorylation correlates to more inhibition of the myosin heads and a decrease in cardiac contraction [102]. In the context of T2DM, we observed an increase in the phosphorylation of Ser-273 and Ser-302 in *db/db* mice compared to the controls. These two sites are targeted by PKC [41]. The third phosphorylation site of cMyBP-C, Ser-282, and the phosphorylation of cardiac troponin I at ser22/23 were not increased in the *db/db* mice, both downstream of PKA (Fig. 3). This differential phosphorylation suggests that the kinase landscape of the heart may be altered in the setting of T2DM-CM.

RNAseq and enrichment analysis of DEGs further showed that upregulated genes were enriched for the GO class “regulation of protein kinase activity.” While we did not observe any significant differences in the transcript levels of various protein kinase genes, alterations at protein levels and protein modifications might affect key molecular events. PKC activation was also observed in diabetic hearts, and PKC inhibitors help preserve cardiac function and improve T2DM-mediated pathologic consequences [108,109]. This supports our data showing that preferential phosphorylation of cMyBP-C at PKC phosphorylation sites mainly results from PKC activation in *db/db* mice hearts.

Our experimental design in this paper is driven by the hypothesis that hyperphosphorylation leads to increased actomyosin interactions and hypercontraction, enhancing relaxation [46,51,110–112], contraction [103,113–115], and calcium responsiveness. This hypothesis

was further supported by our *ex vivo* studies on isolated papillary muscles and cardiomyocytes. Specifically, the skinned papillary muscle from *db/db* mice exhibited greater force of contraction, calcium sensitivity, and rate of force redevelopment. Moreover, individual cardiomyocytes isolated from the ventricles of *db/db* mice showed increases in fractional shortening, contraction velocity, and diastolic relaxation time compared to cardiomyocytes from age-matched WT mice. The expression levels of *Myh6* and *Myh7* from RNA-Seq data indicate that both Myh isoforms displayed an increased expression in db/db hearts; however, the ratio of *Myh6/Myh7* was nominally reduced (Myh6: Myh7 Case/Myh6: Myh7 Control: 0.8) in *db/db* hearts. Similarly, *Mybpc3* displayed a minimal fold change in db/db hearts in RNA-Seq data, suggesting that the resultant hypercontractile property might primarily be caused by a phosphorylation event, not a switch in *Myh* isoforms or an increased level of *Mybpc3* expression. Taken together, these data point toward cMyBP-C hyperphosphorylation-mediated hypercontractility as a potential target for mitigating the pathogenesis of HFpEF in T2DM-CM.

To this end, we tested MYK-461, a small-molecule modulator of cardiac myosin, which was recently approved by the U.S. FDA for treating hypertrophic cardiomyopathy [116–118]. MYK-461 is a potential target of cMyBP-C hyperphosphorylation because it stabilizes actomyosin interactions by allosteric and reversible inhibition of myosin ATPase and reduces contractility [53,119]. Therefore, the ability of MYK-461 to rescue T2DM-induced HFpEF phenotype was validated by using *ex vivo* systems of skinned papillary muscle fibers and isolated cardiomyocytes from *db/db* and WT mice. Results showed that the MYK-461 treatment significantly reduced elevated contractile parameters, namely F_{max}, $pCa_{50,}$ and k_{tr}, in skinned papillary muscle fibers of the *db/db* group compared to WT levels. Similarly, the MYK-461 treatment significantly reduced contractile velocity and diastolic relaxation time in cardiomyocytes isolated from *db/db* mice. Interestingly, MYK-461 did not affect calcium handling in either *db/db* or WT cardiomyocytes, as indicated by the time constant of calcium decay and calcium transient amplitude values.

In conclusion, this study highlights the importance of cMyBP-C hyperphosphorylation and the effects of T2DM on cardiac dysfunction, both *in vivo* and *ex vivo*. Using *ex vivo* model systems, contractile parameters were increased in *db/db* mice compared to the controls but abrogated by administration of MYK-461 *in vitro*, thus ameliorating cardiac dysfunction in T2DM-CM. Future studies will include *in vivo* confirmation of these findings.

4.1. Study limitations

The *db/db* mouse model is a diabetic model with limited clinical findings related to patients with HFpEF. However, the present studies have used this model to understand any changes in cMyBP-C phosphorylation associated with the development of diastolic dysfunction and determine whether myosin inhibitors can improve diabetes-mediated hypercontraction. In addition, our current findings also need further validation in a different diabetic model, such as the Streptozotocin and high-fat diet mouse model, to confirm the hyperphosphorylation of cMyBP-C in T2DM and its association with early signs of HFpEF and diastolic dysfunction. This could be deemed a limitation of this study.

Supplementary Material

Refer to Web version on PubMed Central for supplementary material.

Acknowledgements

Ms. Desai (Predoctoral, 20PRE35120272), Dr. Kumar (Postdoctoral, 834316), and Dr. Green (Postdoctoral, 23POST1019099) were supported by American Heart Association Fellowships. Dr. Sadayappan received funding support from National Institutes of Health grants R01 AR079435, R01 AR079477, R01 AR078001, R01 HL130356, R01 HL105826, R38 HL155775 and R01 HL143490, the American Heart Association 2019 Institutional Undergraduate Student (19UFEL34380251) and Transformation (19TPA34830084 and 945748) awards, the PLN Foundation (PLN crazy idea) and the Leducq Foundation (Transatlantic Network 18CVD01, PLN-CURE).

Declaration of competing interest

The authors declare the following financial interests/personal relationships which may be considered as potential competing interests: Sakthivel Sadayappan reports financial support was provided by University of Cincinnati. Sakthivel Sadayappan reports a relationship with American Heart Association Inc. that includes: board membership. Sakthivel Sadayappan has patent #US Provisional Application No. 63/271482 filed on October 25, 2021 Full application CIN 0351/10738-995 was filed on October 22, 2022. UC Ref: 2022-30 Title: Molecular therapeutics to treat left ventricular hypertrophy, hypertrophic cardiomyopathy and heart failure caused by *MYBPC3* gene mutations Inventors: Sadayappan pending to 63/271482. Dr. Sadayappan is Visiting Professor, Indian Institute of Technology, Chennai, India, and provides consulting and collaborative research studies to the Leducq Foundation (CURE-PLAN), Red Saree Inc., Greater Cincinnati Tamil Sangam, Novo Nordisk, Pfizer, AavantiBio, Affinia Therapeutics Inc., Cardiocare Genetics - Cosmogene Skincare Pvt Ltd, AstraZeneca, MyoKardia, Merck and Amgen, but such work is unrelated to the content of this article. A.G. J. is a member of the Scientific Advisory Board of Gen1E Lifesciences, USA.

References

[1]. McHugh K, DeVore AD, Wu J, Matsouaka RA, Fonarow GC, Heidenreich PA, et al. Heart failure with preserved ejection fraction and diabetes: JACC state-of-the-art review. J Am Coll Cardiol 2019;73:602–11. [PubMed: 30732715]

[2]. Dunlay SM, Roger VL, Redfield MM. Epidemiology of heart failure with preserved ejection fraction. Nat Rev Cardiol 2017;14:591–602. [PubMed: 28492288]

[3]. Shah SJ, Voors AA, McMurray JJV, Kitzman DW, Viethen T, Bomfim Wirtz A, et al. Effect of Neladenoson Bialanate on exercise capacity among patients with heart failure with preserved ejection fraction: a randomized clinical trial. JAMA 2019;321:2101–12. [PubMed: 31162568]

[4]. Owan TE, Hodge DO, Herges RM, Jacobsen SJ, Roger VL, Redfield MM. Trends in prevalence and outcome of heart failure with preserved ejection fraction. N Engl J Med 2006;355:251–9. [PubMed: 16855265]

[5]. Zile MR, Brutsaert DL. New concepts in diastolic dysfunction and diastolic heart failure: part I: diagnosis, prognosis, and measurements of diastolic function. Circulation 2002;105:1387–93. [PubMed: 11901053]

[6]. Paulus WJ, Tschope C. A novel paradigm for heart failure with preserved ejection fraction: comorbidities drive myocardial dysfunction and remodeling through coronary microvascular endothelial inflammation. J Am Coll Cardiol 2013;62: 263–71. [PubMed: 23684677]

[7]. Mentz RJ, Kelly JP, von Lueder TG, Voors AA, Lam CS, Cowie MR, et al. Noncardiac comorbidities in heart failure with reduced versus preserved ejection fraction. J Am Coll Cardiol 2014;64:2281–93. [PubMed: 25456761]

[8]. Varnado S, Ali HR, Trachtenberg B. Medical therapy for heart failure with preserved ejection fraction. Methodist Debakey Cardiovasc J 2022;18:17–26.

[9]. Bertoni AG, Hundley WG, Massing MW, Bonds DE, Burke GL, Goff DC Jr. Heart failure prevalence, incidence, and mortality in the elderly with diabetes. Diabetes Care 2004;27:699–703. [PubMed: 14988288]

[10]. MacDonald MR, Petrie MC, Varyani F, Ostergren J, Michelson EL, Young JB, et al. Impact of diabetes on outcomes in patients with low and preserved ejection fraction heart failure: an analysis of the candesartan in heart failure: assessment of reduction in mortality and morbidity (CHARM) programme. Eur Heart J 2008; 29:1377–85. [PubMed: 18413309]

[11]. Sarma S, Mentz RJ, Kwasny MJ, Fought AJ, Huffman M, Subacius H, et al. Association between diabetes mellitus and post-discharge outcomes in patients hospitalized with heart failure: findings from the EVEREST trial. Eur J Heart Fail 2013;15:194–202. [PubMed: 23059198]

[12]. Savji N, Meijers WC, Bartz TM, Bhambhani V, Cushman M, Nayor M, et al. The Association of Obesity and Cardiometabolic Traits with Incident HFpEF and HFrEF. JACC Heart Fail 2018;6:701–9. [PubMed: 30007554]

[13]. Kristensen SL, Mogensen UM, Jhund PS, Petrie MC, Preiss D, Win S, et al. Clinical and echocardiographic characteristics and cardiovascular outcomes according to diabetes status in patients with heart failure and preserved ejection fraction: a report From the I-preserve trial (Irbesartan in heart failure with preserved ejection fraction). Circulation 2017;135:724–35. [PubMed: 28052977]

[14]. Mekhaimar M, Al Mohannadi M, Dargham S, Al Suwaidi J, Jneid H, Abi Khalil C. Diabetes outcomes in heart failure patients with hypertrophic cardiomyopathy. Front Physiol 2022;13:976315.

[15]. Rowley WR, Bezold C, Arikan Y, Byrne E, Krohe S. Diabetes 2030: insights from yesterday, Today, and future trends. Popul Health Manag 2017;20:6–12. [PubMed: 27124621]

[16]. Jex N, Chowdhary A, Thirunavukarasu S, Procter H, Sengupta A, Natarajan P, et al. Coexistent diabetes is associated with the presence of adverse phenotypic features in patients with hypertrophic cardiomyopathy. Diabetes Care 2022;45: 1852–62. [PubMed: 35789379]

[17]. Tan Y, Zhang Z, Zheng C, Wintergerst KA, Keller BB, Cai L. Mechanisms of diabetic cardiomyopathy and potential therapeutic strategies: preclinical and clinical evidence. Nat Rev Cardiol 2020;17:585–607. [PubMed: 32080423]

[18]. Seferovic PM, Paulus WJ. Clinical diabetic cardiomyopathy: a two-faced disease with restrictive and dilated phenotypes. Eur Heart J 2015;36(1718–27) [1727a–1727c].

[19]. Rubler S, Dlugash J, Yuceoglu YZ, Kumral T, Branwood AW, Grishman A. New type of cardiomyopathy associated with diabetic glomerulosclerosis. Am J Cardiol 1972;30:595–602. [PubMed: 4263660]

[20]. Meagher P, Adam M, Civitarese R, Bugyei-Twum A, Connelly KA. Heart failure with preserved ejection fraction in diabetes: mechanisms and management. Can J Cardiol 2018;34:632–43. [PubMed: 29731023]

[21]. Redfield MM, Jacobsen SJ, Burnett JC Jr, Mahoney DW, Bailey KR, Rodeheffer RJ. Burden of systolic and diastolic ventricular dysfunction in the community: appreciating the scope of the heart failure epidemic. JAMA 2003; 289:194–202. [PubMed: 12517230]

[22]. Kavey RE, Allada V, Daniels SR, Hayman LL, McCrindle BW, Newburger JW, et al. Cardiovascular risk reduction in high-risk pediatric patients: a scientific statement from the American Heart Association expert panel on population and prevention science; the councils on cardiovascular disease in the Young, epidemiology and prevention, nutrition, physical activity and metabolism, high blood pressure research, cardiovascular nursing, and the kidney in heart disease; and the interdisciplinary working group on quality of care and outcomes research. J Cardiovasc Nurs 2007;22:218–53. [PubMed: 17545824]

[23]. Shah AS, Khoury PR, Dolan LM, Ippisch HM, Urbina EM, Daniels SR, et al. The effects of obesity and type 2 diabetes mellitus on cardiac structure and function in adolescents and young adults. Diabetologia 2011;54:722–30. [PubMed: 21085926]

[24]. Bjornstad P, Truong U, Dorosz JL, Cree-Green M, Baumgartner A, Coe G, et al. Cardiopulmonary dysfunction and adiponectin in adolescents with type 2 diabetes. J Am Heart Assoc 2016;5:e002804. [PubMed: 26994128]

[25]. Levitt Katz L, Gidding SS, Bacha F, Hirst K, McKay S, Pyle L, et al. Alterations in left ventricular, left atrial, and right ventricular structure and function to cardiovascular risk factors in adolescents with type 2 diabetes participating in the TODAY clinical trial. Pediatr Diabetes 2015;16:39–47. [PubMed: 24450390]

[26]. Nadeau KJ, Zeitler PS, Bauer TA, Brown MS, Dorosz JL, Draznin B, et al. Insulin resistance in adolescents with type 2 diabetes is associated with impaired exercise capacity. J Clin Endocrinol Metab 2009;94:3687–95. [PubMed: 19584191]

[27]. Tamborlane WV, Haymond MW, Dunger D, Shankar R, Gubitosi-Klug R, Bethin K, et al. Expanding treatment options for youth with type 2 diabetes: current problems and proposed solutions: a white paper From the NICHD diabetes working group. Diabetes Care 2016;39:323–9. [PubMed: 26908928]

[28]. Lopaschuk GD, Verma S. Mechanisms of cardiovascular benefits of sodium glucose co-transporter 2 (SGLT2) inhibitors: a state-of-the-art review. JACC Basic Transl Sci 2020;5:632–44. [PubMed: 32613148]

[29]. Verma S, Garg A, Yan AT, Gupta AK, Al-Omran M, Sabongui A, et al. Effect of Empagliflozin on left ventricular mass and diastolic function in individuals with diabetes: an important clue to the EMPA-REG OUTCOME trial? Diabetes Care 2016;39:e212–3. [PubMed: 27679584]

[30]. Packer M Autophagy stimulation and intracellular sodium reduction as mediators of the cardioprotective effect of sodium-glucose cotransporter 2 inhibitors. Eur J Heart Fail 2020;22:618–28. [PubMed: 32037659]

[31]. Chen S, Coronel R, Hollmann MW, Weber NC, Zuurbier CJ. Direct cardiac effects of SGLT2 inhibitors. Cardiovasc Diabetol 2022;21:45. [PubMed: 35303888]

[32]. Talha KM, Anker SD, Butler J. SGLT-2 inhibitors in heart failure: a review of current evidence. Int J Heart Fail 2023;5:82–90. [PubMed: 37180562]

[33]. Neal B, Perkovic V, Mahaffey KW, de Zeeuw D, Fulcher G, Erondu N, et al. Canagliflozin and cardiovascular and renal events in type 2 diabetes. N Engl J Med 2017;377:644–57. [PubMed: 28605608]

[34]. Wiviott SD, Raz I, Bonaca MP, Mosenzon O, Kato ET, Cahn A, et al. Dapagliflozin and cardiovascular outcomes in type 2 diabetes. N Engl J Med 2019;380:347–57. [PubMed: 30415602]

[35]. Cannon CP, Pratley R, Dagogo-Jack S, Mancuso J, Huyck S, Masiukiewicz U, et al. Cardiovascular outcomes with Ertugliflozin in type 2 diabetes. N Engl J Med 2020;383:1425–35. [PubMed: 32966714]

[36]. Bhatt DL, Szarek M, Steg PG, Cannon CP, Leiter LA, McGuire DK, et al. Sotagliflozin in patients with diabetes and recent worsening heart failure. N Engl J Med 2021;384:117–28. [PubMed: 33200892]

[37]. Butler J, Packer M, Filippatos G, Ferreira JP, Zeller C, Schnee J, et al. Effect of empagliflozin in patients with heart failure across the spectrum of left ventricular ejection fraction. Eur Heart J 2022;43:416–26. [PubMed: 34878502]

[38]. Whitten AE, Jeffries CM, Harris SP, Trewhella J. Cardiac myosin-binding protein C decorates F-actin: implications for cardiac function. Proc Natl Acad Sci U S A 2008;105:18360–5. [PubMed: 19011110]

[39]. Sadayappan S, de Tombe PP. Cardiac myosin binding protein-C: redefining its structure and function. Biophys Rev 2012;4:93–106. [PubMed: 22707987]

[40]. Lynch TLt, Kumar M, McNamara JW, Kuster DWD, Sivaguru M, Singh RR, et al. Amino terminus of cardiac myosin binding protein-C regulates cardiac contractility. J Mol Cell Cardiol 2021;156:33–44. [PubMed: 33781820]

[41]. Sadayappan S, Gulick J, Osinska H, Barefield D, Cuello F, Avkiran M, et al. A critical function for Ser-282 in cardiac myosin binding protein-C phosphorylation and cardiac function. Circ Res 2011;109:141–50. [PubMed: 21597010]

[42]. Barefield D, Sadayappan S. Phosphorylation and function of cardiac myosin binding protein-C in health and disease. J Mol Cell Cardiol 2010;48:866–75. [PubMed: 19962384]

[43]. McNamara JW, Singh RR, Sadayappan S. Cardiac myosin binding protein-C phosphorylation regulates the super-relaxed state of myosin. Proc Natl Acad Sci U S A 2019;116:11731–6. [PubMed: 31142654]

[44]. Kuster DW, Bawazeer AC, Zaremba R, Goebel M, Boontje NM, van der Velden J. Cardiac myosin binding protein C phosphorylation in cardiac disease. J Muscle Res Cell Motil 2012;33:43–52. [PubMed: 22127559]

[45]. Rosas PC, Liu Y, Abdalla MI, Thomas CM, Kidwell DT, Dusio GF, et al. Phosphorylation of cardiac myosin-binding protein-C is a critical mediator of diastolic function. Circ Heart Fail 2015;8:582–94. [PubMed: 25740839]

[46]. Hartzell HC, Glass DB. Phosphorylation of purified cardiac muscle C-protein by purified cAMP-dependent and endogenous Ca2+−calmodulin-dependent protein kinases. J Biol Chem 1984;259:15587–96. [PubMed: 6549009]

[47]. Schlender KK, Bean LJ. Phosphorylation of chicken cardiac C-protein by calcium/calmodulin-dependent protein kinase II. J Biol Chem 1991;266:2811–7. [PubMed: 1671569]

[48]. Kumar M, Haghighi K, Kranias EG, Sadayappan S. Phosphorylation of cardiac myosin-binding protein-C contributes to calcium homeostasis. J Biol Chem 2020; 295:11275–91. [PubMed: 32554466]

[49]. Mamidi R, Li J, Gresham KS, Stelzer JE. Cardiac myosin binding protein-C: a novel sarcomeric target for gene therapy. Pflugers Arch 2014;466:225–30. [PubMed: 24310821]

[50]. Gautel M, Zuffardi O, Freiburg A, Labeit S. Phosphorylation switches specific for the cardiac isoform of myosin binding protein-C: a modulator of cardiac contraction? EMBO J 1995;14:1952–60. [PubMed: 7744002]

[51]. McClellan G, Weisberg A, Winegrad S. cAMP can raise or lower cardiac actomyosin ATPase activity depending on alpha-adrenergic activity. Am J Physiol 1994;267:H431–42. [PubMed: 7915082]

[52]. Basile JN. Antihypertensive therapy, new-onset diabetes, and cardiovascular disease. Int J Clin Pract 2009;63:656–66. [PubMed: 19220522]

[53]. Kawas RF, Anderson RL, Ingle SRB, Song Y, Sran AS, Rodriguez HM. A small-molecule modulator of cardiac myosin acts on multiple stages of the myosin chemomechanical cycle. J Biol Chem 2017;292:16571–7. [PubMed: 28808052]

[54]. Hall ME, Maready MW, Hall JE, Stec DE. Rescue of cardiac leptin receptors in db/db mice prevents myocardial triglyceride accumulation. Am J Physiol Endocrinol Metab 2014;307:E316–25. [PubMed: 24939734]

[55]. Burke SJ, Batdorf HM, Burk DH, Noland RC, Eder AE, Boulos MS, et al. Db/db mice exhibit features of human type 2 diabetes that are not present in weight-matched C57BL/6J mice fed a Western diet. J Diabetes Res 2017;2017:8503754.

[56]. Alex L, Russo I, Holoborodko V, Frangogiannis NG. Characterization of a mouse model of obesity-related fibrotic cardiomyopathy that recapitulates features of human heart failure with preserved ejection fraction. Am J Physiol Heart Circ Physiol 2018;315:H934–49. [PubMed: 30004258]

[57]. Belke DD, Severson DL. Diabetes in mice with monogenic obesity: the db/db mouse and its use in the study of cardiac consequences. Methods Mol Biol 2012; 933:47–57. [PubMed: 22893400]

[58]. Otto M, Brabenec L, Muller M, Kintrup S, Hellenthal KEM, Holtmeier R, et al. Development of heart failure with preserved ejection fraction in type 2 diabetic mice is ameliorated by preserving vascular function. Life Sci 2021;284:119925.

[59]. de Lucia C, Wallner M, Eaton DM, Zhao H, Houser SR, Koch WJ. Echocardiographic strain analysis for the early detection of left ventricular systolic/diastolic dysfunction and Dyssynchrony in a mouse model of physiological aging. J Gerontol A Biol Sci Med Sci 2019;74:455–61. [PubMed: 29917053]

[60]. Koch SE, Gao X, Haar L, Jiang M, Lasko VM, Robbins N, et al. Probenecid: novel use as a non-injurious positive inotrope acting via cardiac TRPV2 stimulation. J Mol Cell Cardiol 2012;53:134–44. [PubMed: 22561103]

[61]. Koch SE, Mann A, Jones S, Robbins N, Alkhattabi A, Worley MC, et al. Transient receptor potential vanilloid 2 function regulates cardiac hypertrophy via stretch-induced activation. J Hypertens 2017;35:602–11. [PubMed: 28009703]

[62]. Barefield DY, McNamara JW, Lynch TL, Kuster DWD, Govindan S, Haar L, et al. Ablation of the calpain-targeted site in cardiac myosin binding protein-C is cardioprotective during ischemia-reperfusion injury. J Mol Cell Cardiol 2019;129: 236–46. [PubMed: 30862451]

[63]. Kuster DWD, Lynch TL, Barefield DY, Sivaguru M, Kuffel G, Zilliox MJ, et al. Altered C10 domain in cardiac myosin binding protein-C results in hypertrophic cardiomyopathy. Cardiovasc Res 2019;115:1986–97. [PubMed: 31050699]

[64]. Langmead B, Salzberg SL. Fast gapped-read alignment with bowtie 2. Nat Methods 2012;9:357–9. [PubMed: 22388286]

[65]. Li B, Dewey CN. RSEM: accurate transcript quantification from RNA-Seq data with or without a reference genome. BMC Bioinformatics 2011;12:323. [PubMed: 21816040]

[66]. Love MI, Huber W, Anders S. Moderated estimation of fold change and dispersion for RNA-seq data with DESeq2. Genome Biol 2014;15:550. [PubMed: 25516281]

[67]. Chen J, Bardes EE, Aronow BJ, Jegga AG. ToppGene suite for gene list enrichment analysis and candidate gene prioritization. Nucleic Acids Res 2009;37:W305–11. [PubMed: 19465376]

[68]. Ait-Mou Y, Hsu K, Farman GP, Kumar M, Greaser ML, Irving TC, et al. Titin strain contributes to the Frank–Starling law of the heart by structural rearrangements of both thin- and thick-filament proteins. Proc Natl Acad Sci U S A 2016;113: 2306–11. [PubMed: 26858417]

[69]. Bidwell PA, Haghighi K, Kranias EG. The antiapoptotic protein HAX-1 mediates half of phospholamban's inhibitory activity on calcium cycling and contractility in the heart. J Biol Chem 2018;293:359–67. [PubMed: 29150445]

[70]. Woody MS, Greenberg MJ, Barua B, Winkelmann DA, Goldman YE, Ostap EM. Positive cardiac inotrope omecamtiv mecarbil activates muscle despite suppressing the myosin working stroke. Nat Commun 2018;9:3838. [PubMed: 30242219]

[71]. Semeniuk LM, Kryski AJ, Severson DL. Echocardiographic assessment of cardiac function in diabetic db/db and transgenic db/db-hGLUT4 mice. Am J Physiol Heart Circ Physiol 2002;283:H976–82. [PubMed: 12181126]

[72]. Kunst G, Kress KR, Gruen M, Uttenweiler D, Gautel M, Fink RH. Myosin binding protein C, a phosphorylation-dependent force regulator in muscle that controls the attachment of myosin heads by its interaction with myosin S2. Circ Res 2000; 86:51–8. [PubMed: 10625305]

[73]. Salhi HE, Shettigar V, Salyer L, Sturgill S, Brundage EA, Robinett J, et al. The lack of troponin I Ser-23/24 phosphorylation is detrimental to in vivo cardiac function and exacerbates cardiac disease. J Mol Cell Cardiol 2023;176:84–96. [PubMed: 36724829]

[74]. Green EM, Wakimoto H, Anderson RL, Evanchik MJ, Gorham JM, Harrison BC, et al. A small-molecule inhibitor of sarcomere contractility suppresses hypertrophic cardiomyopathy in mice. Science 2016;351:617–21. [PubMed: 26912705]

[75]. Mathers CD, Loncar D. Projections of global mortality and burden of disease from 2002 to 2030. PLoS Med 2006;3:e442. [PubMed: 17132052]

[76]. Ng AC, Auger D, Delgado V, van Elderen SG, Bertini M, Siebelink HM, et al. Association between diffuse myocardial fibrosis by cardiac magnetic resonance contrast-enhanced T1 mapping and subclinical myocardial dysfunction in diabetic patients: a pilot study. Circ Cardiovasc Imaging 2012;5:51–9. [PubMed: 22135399]

[77]. From AM, Scott CG, Chen HH. The development of heart failure in patients with diabetes mellitus and pre-clinical diastolic dysfunction a population-based study. J Am Coll Cardiol 2010;55:300–5. [PubMed: 20117433]

[78]. Gu J, Fan YQ, Zhang JF, Wang CQ. Association of hemoglobin A1c variability and the incidence of heart failure with preserved ejection fraction in patients with type 2 diabetes mellitus and arterial hypertension. Hellenic J Cardiol 2018;59: 91–7. [PubMed: 28818638]

[79]. Dhingra A, Garg A, Kaur S, Chopra S, Batra JS, Pandey A, et al. Epidemiology of heart failure with preserved ejection fraction. Curr Heart Fail Rep 2014;11: 354–65. [PubMed: 25224319]

[80]. Nichols GA, Gullion CM, Koro CE, Ephross SA, Brown JB. The incidence of congestive heart failure in type 2 diabetes: an update. Diabetes Care 2004;27: 1879–84. [PubMed: 15277411]

[81]. Dunlay SM, Givertz MM, Aguilar D, Allen LA, Chan M, Desai AS, et al. Type 2 diabetes mellitus and heart failure: a scientific statement From the American Heart Association and the Heart Failure Society of America. Circulation 2019; 140:e294–324. [PubMed: 31167558]

[82]. Seferovic PM, Petrie MC, Filippatos GS, Anker SD, Rosano G, Bauersachs J, et al. Type 2 diabetes mellitus and heart failure: a position statement from the heart failure Association of the European Society of cardiology. Eur J Heart Fail 2018; 20:853–72. [PubMed: 29520964]

[83]. Authors M, Task Force L, Ryden PJ, Grant SD, Anker C, Cosentino Berne F, et al. ESC guidelines on diabetes, pre-diabetes, and cardiovascular diseases developed in collaboration with the EASD: the Task Force on diabetes, pre-diabetes, and cardiovascular diseases of the European Society of Cardiology (ESC) and developed in collaboration with the European Association for the Study of diabetes (EASD). Eur Heart J 2013;34:3035–87. [PubMed: 23996285]

[84]. Yancy CW, Jessup M, Bozkurt B, Butler J, Casey DE Jr, Drazner MH, et al. 2013 ACCF/AHA guideline for the management of heart failure: a report of the American College of Cardiology Foundation/American Heart Association Task Force on practice guidelines. J Am Coll Cardiol 2013;62:e147–239. [PubMed: 23747642]

[85]. Sharma K, Kass DA. Heart failure with preserved ejection fraction: mechanisms, clinical features, and therapies. Circ Res 2014;115:79–96. [PubMed: 24951759]

[86]. Butler J, Lam CSP, Anstrom KJ, Ezekowitz J, Hernandez AF, O'Connor CM, et al. Rationale and design of the VITALITY-HFpEF trial. Circ Heart Fail 2019;12: e005998. [PubMed: 31096775]

[87]. Patel RB, Vaduganathan M, Felker GM, Butler J, Redfield MM, Shah SJ. Physical activity, quality of life, and biomarkers in atrial fibrillation and heart failure with preserved ejection fraction (from the NEAT-HFpEF trial). Am J Cardiol 2019;123: 1660–6. [PubMed: 30876658]

[88]. Chamsi-Pasha MA, Zhan Y, Debs D, Shah DJ. CMR in the evaluation of diastolic dysfunction and phenotyping of HFpEF: current role and future perspectives. JACC Cardiovasc Imaging 2020;13:283–96. [PubMed: 31202753]

[89]. Reil JC, Hohl M, Reil GH, Granzier HL, Kratz MT, Kazakov A, et al. Heart rate reduction by if-inhibition improves vascular stiffness and left ventricular systolic and diastolic function in a mouse model of heart failure with preserved ejection fraction. Eur Heart J 2013;34:2839–49. [PubMed: 22833515]

[90]. Hamdani N, Hervent AS, Vandekerckhove L, Matheeussen V, Demolder M, Baerts L, et al. Left ventricular diastolic dysfunction and myocardial stiffness in diabetic mice is attenuated by inhibition of dipeptidyl peptidase 4. Cardiovasc Res 2014;104:423–31. [PubMed: 25341892]

[91]. Mori J, Patel VB, Abo Alrob O, Basu R, Altamimi T, Desaulniers J, et al. Angiotensin 1–7 ameliorates diabetic cardiomyopathy and diastolic dysfunction in db/db mice by reducing lipotoxicity and inflammation. Circ Heart Fail 2014;7: 327–39. [PubMed: 24389129]

[92]. Mishra S, Kass DA. Cellular and molecular pathobiology of heart failure with preserved ejection fraction. Nat Rev Cardiol 2021;18:400–23. [PubMed: 33432192]

[93]. Quttainah M, Raveendran VV, Saleh S, Parhar R, Aljoufan M, Moorjani N, et al. Transcriptomal insights of heart failure from normality to recovery. Biomolecules 2022:12. [PubMed: 36671397]

[94]. Saw EL, Ramachandran S, Valero-Munoz M, Sam F. Skeletal muscle (dys)function in heart failure with preserved ejection fraction. Curr Opin Cardiol 2021;36: 219–26. [PubMed: 33394707]

[95]. Biesemann N, Mendler L, Wietelmann A, Hermann S, Schafers M, Kruger M, et al. Myostatin regulates energy homeostasis in the heart and prevents heart failure. Circ Res 2014;115:296–310. [PubMed: 24807786]

[96]. Chen P, Liu Z, Luo Y, Chen L, Li S, Pan Y, et al. Predictive value of serum myostatin for the severity and clinical outcome of heart failure. Eur J Intern Med 2019;64:33–40. [PubMed: 31056368]

[97]. Sakane K, Kanzaki Y, Tsuda K, Maeda D, Sohmiya K, Hoshiga M. Disproportionately low BNP levels in patients of acute heart failure with preserved vs. reduced ejection fraction. Int J Cardiol 2021;327:105–10. [PubMed: 33279592]

[98]. Maisel AS, McCord J, Nowak RM, Hollander JE, Wu AH, Duc P, et al. Bedside B-type natriuretic peptide in the emergency diagnosis of heart failure with reduced or preserved ejection fraction. Results from the breathing not properly multinational study. J Am Coll Cardiol 2003;41:2010–7. [PubMed: 12798574]

[99]. Bachmann KN, Gupta DK, Xu M, Brittain E, Farber-Eger E, Arora P, et al. Unexpectedly low natriuretic peptide levels in patients with heart failure. JACC Heart Fail 2021;9:192–200. [PubMed: 33422435]

[100]. Schiattarella GG, Rodolico D, Hill JA. Metabolic inflammation in heart failure with preserved ejection fraction. Cardiovasc Res 2021;117:423–34. [PubMed: 32666082]

[101]. Mohamed AS, Dignam JD, Schlender KK. Cardiac myosin-binding protein C (MyBP-C): identification of protein kinase a and protein kinase C phosphorylation sites. Arch Biochem Biophys 1998;358:313–9. [PubMed: 9784245]

[102]. Sadayappan S, Gulick J, Osinska H, Martin LA, Hahn HS, Dorn GW 2nd, et al. Cardiac myosin-binding protein-C phosphorylation and cardiac function. Circ Res 2005;97:1156–63. [PubMed: 16224063]

[103]. Garvey JL, Kranias EG, Solaro RJ. Phosphorylation of C-protein, troponin I and phospholamban in isolated rabbit hearts. Biochem J 1988;249:709–14. [PubMed: 2895634]

[104]. Gruen M, Gautel M. Mutations in beta-myosin S2 that cause familial hypertrophic cardiomyopathy (FHC) abolish the interaction with the regulatory domain of myosin-binding protein-C. J Mol Biol 1999;286:933–49. [PubMed: 10024460]

[105]. Weisberg A, Winegrad S. Alteration of myosin cross bridges by phosphorylation of myosin-binding protein C in cardiac muscle. Proc Natl Acad Sci U S A 1996;93: 8999–9003. [PubMed: 8799143]

[106]. Winegrad S Cardiac myosin binding protein C. Circ Res 1999;84:1117–26. [PubMed: 10347086]

[107]. Winegrad S Myosin binding protein C, a potential regulator of cardiac contractility. Circ Res 2000;86:6–7. [PubMed: 10625298]

[108]. Connelly KA, Kelly DJ, Zhang Y, Prior DL, Advani A, Cox AJ, et al. Inhibition of protein kinase C-beta by ruboxistaurin preserves cardiac function and reduces extracellular matrix production in diabetic cardiomyopathy. Circ Heart Fail 2009; 2:129–37. [PubMed: 19808328]

[109]. Durpes MC, Morin C, Paquin-Veillet J, Beland R, Pare M, Guimond MO, et al. PKC-beta activation inhibits IL-18-binding protein causing endothelial dysfunction and diabetic atherosclerosis. Cardiovasc Res 2015;106:303–13. [PubMed: 25808972]

[110]. Hartzell HC. Effects of phosphorylated and unphosphorylated C-protein on cardiac actomyosin ATPase. J Mol Biol 1985;186:185–95. [PubMed: 2934553]

[111]. Hofmann PA, Greaser ML, Moss RL. C-protein limits shortening velocity of rabbit skeletal muscle fibres at low levels of Ca2+ activation. J Physiol 1991;439: 701–15. [PubMed: 1895247]

[112]. Hofmann PA, Hartzell HC, Moss RL. Alterations in Ca2+ sensitive tension due to partial extraction of C-protein from rat skinned cardiac myocytes and rabbit skeletal muscle fibers. J Gen Physiol 1991;97:1141–63. [PubMed: 1678777]

[113]. Hofmann PA, Lange JH 3rd. Effects of phosphorylation of troponin I and C protein on isometric tension and velocity of unloaded shortening in skinned single cardiac myocytes from rats. Circ Res 1994;74:718–26. [PubMed: 8137507]

[114]. Wattanapermpool J, Guo X, Solaro RJ. The unique amino-terminal peptide of cardiac troponin I regulates myofibrillar activity only when it is phosphorylated. J Mol Cell Cardiol 1995;27:1383–91. [PubMed: 7473784]

[115]. Kentish JC, McCloskey DT, Layland J, Palmer S, Leiden JM, Martin AF, et al. Phosphorylation of troponin I by protein kinase a accelerates relaxation and crossbridge cycle kinetics in mouse ventricular muscle. Circ Res 2001;88: 1059–65. [PubMed: 11375276]

[116]. Hameed I, Siddiqui OM, Samad SA. MAVACAMTEN: a door that has opened in the treatment of hypertrophic cardiomyopathy. J Pak Med Assoc 2023;73:446–7. [PubMed: 36800755]

[117]. Zatorski N, Sobie EA, Schlessinger A. Mavacamten improves symptoms in obstructive hypertrophic cardiomyopathy patients. Trends Pharmacol Sci 2023; 44:318–9. [PubMed: 36914446]

[118]. Schenk A, Fields N. Mavacamten-a targeted therapy for hypertrophic cardiomyopathy. J Cardiovasc Pharmacol 2023;81:317–26. [PubMed: 36878205]

[119]. Rohde JA, Roopnarine O, Thomas DD, Muretta JM. Mavacamten stabilizes an autoinhibited state of two-headed cardiac myosin. Proc Natl Acad Sci U S A 2018; 115:E7486–94. [PubMed: 30018063]

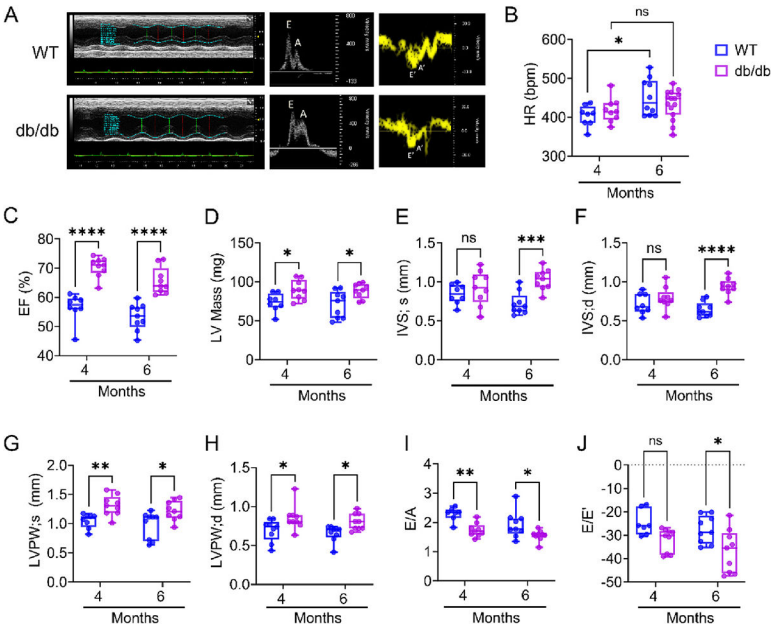

Fig. 1.

Echocardiographic analysis of *db/db* mice at four and six months of age. (A) Representative M-Mode (left), Power Doppler (middle), and Tissue Doppler (right) echocardiographic images of WT (top) and *db/db* (bottom) mouse hearts. Echocardiographic assessment comparing(B) Heart Rate, (C) Ejection fraction, (D) LV Mass, (E) interventricular septal thickness at end-systole (IVS;s) and F) end-diastole (IVS;d), (G) Left ventricular posterior wall thickness during systole (LVPW;s), and (H) diastole (LVPW;d) of WT and *db/db* mice. Mitral inflow measurements included peak E and A waves to derive (I) *E*-to-A ratio (E/A) and (J) E to E′ ratio (E/E′) comparing WT and *db/db* mice. Echocardiography data are expressed as mean ± S.E.M. (error bars). Statistical analyses were performed in all groups by two-way ANOVA, followed by Sidak's multiple-comparison test to compare WT and *db/db* mice at 4 and 6 months of age; $n = 8$ for WT and $n = 9$ for *db/db*. $^{ns}P > 0.05$, $^{*}P \leq 0.05$, $^{**}P \leq 0.01$ and $^{***}P \leq 0.001$ *db/db vs* WT.

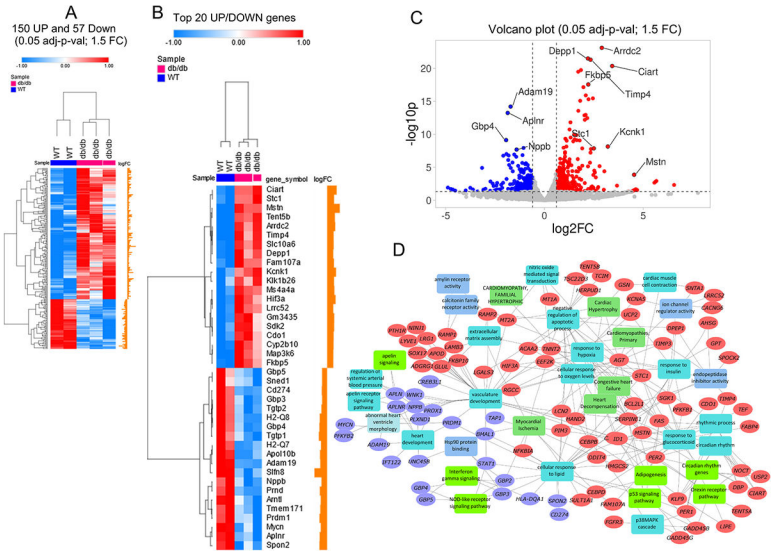

Fig. 2.

RNA-Seq analysis in six-month-old WT *versus db/db* mice hearts. (A) Gene cluster heatmap showing clusters of differentially expressed genes (DEGs) in wild-type (WT) *versus db/db* mice. A heatmap was generated using Morpheus. (B) Heatmap representing the top twenty upregulated and downregulated genes in *db/db* hearts. Blue indicates down-regulated genes, while red indicates up-regulated genes. (C) Volcano plot illustrating upregulated (150) and downregulated (57) genes in six-month-old *db/db* mice hearts (WT ($n = 2$) *vs. db/db* ($n = 3$) (Fold change cutoff 1.5, Adjusted *P*-Value <0.05). (D) Network representation of significantly enriched pathways/processes associated with differentially expressed genes. Rectangular nodes are the enriched biological processes, pathways, and phenotypes. Functional enrichment was performed using the ToppFun application of the ToppGene Suite, and network visualization was done using the Cytoscape application.

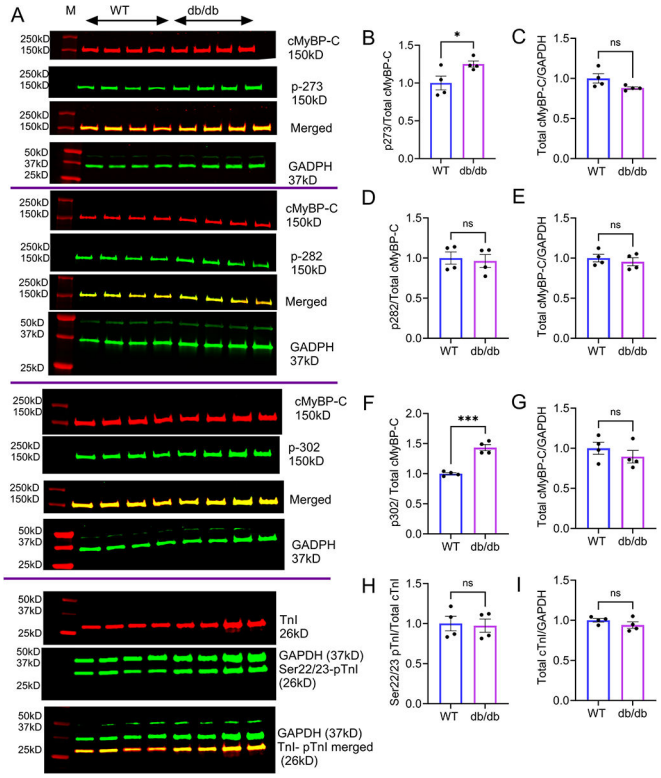

Fig. 3.

T2DM-CM is associated with hyperphosphorylation of cMyBP-C. (A) Representative Western Blot images cMyBP-C phosphorylation (Ser-273, Ser-282, and Ser-302) and cTnI phosphorylation (Ser22/23) in WT and *db/db* mice. (B–I) Densitometric bar graphs of cMyBP-C phosphorylation, cTnI phosphorylation, total cMyBP-C, and cTnI protein levels. The bar graphs in the middle represent the average cMyBP-C and cTnI phosphorylation normalized to their respective total protein. The bar graphs in the right panel represent total cMyBP-C and cTnI normalized to GAPDH. Solid purple lines separate individual whole blots. Phosphorylation and total expression of cMyBP-C and cTnI proteins were detected by dual-color Western blotting using two IR fluorophores. Both phospho-specific and pan-specific blot intensities were determined using Fiji software (NIH). M stands for Protein Marker (All blue). Proteins were extracted from the whole-heart lysate of 6-month-old mice. nsP > 0.05, *P ≤ 0.05 and ***P ≤ 0.001 *db/db vs* WT. Immunoblotting data are expressed as mean ± S.E.M. of band intensity, and statistical analyses were performed in all groups by Unpaired *t*-test to compare WT and *db/db* mice at 6 months of age; $n = 4$ hearts/group.

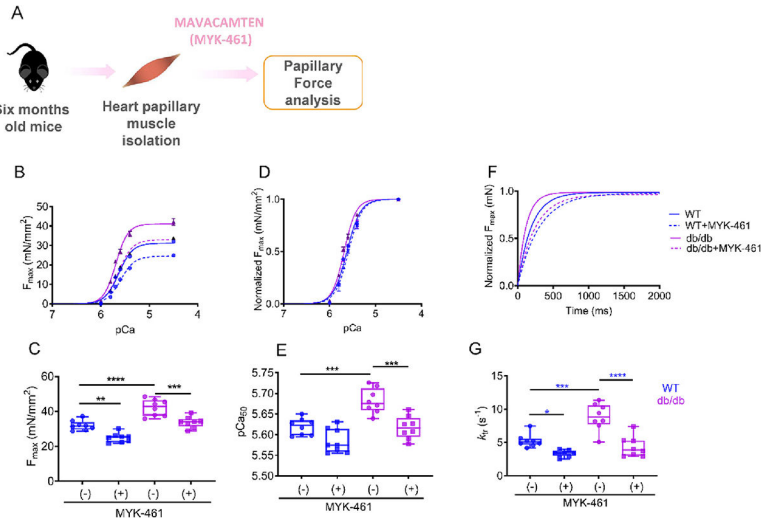

Fig. 4.

Increased maximal pCa-force on skinned papillary muscle fibers of *db/db* mice. (A) Experimental plans for measuring papillary muscle contractility *in vitro*. (B–C) pCa-force relationship and maximal force at pCa 5.5 with (+) and without (−) Mavacamten in WT controls and *db/db* mice at six months of age. The (−) MYK-461 group was treated with an equal volume of the vehicle, DMSO. (D–E) pCa-force relationship and (F–G) k_{tr} values across WT and *db/db* fibers in the presence and absence of MYK-461. ^{ns}P > 0.05, *P ≤ 0.05, **P ≤ 0.01, ***P ≤ 0.001 and ****$P \leq 0.0001$ *db/db vs.* WT. Data are expressed as mean ± SD (n = 8 fibers/3 hearts), and statistical analyses were performed in all groups by ordinary one-way ANOVA, followed by Tukey's multiple comparison test with single pooled variance.

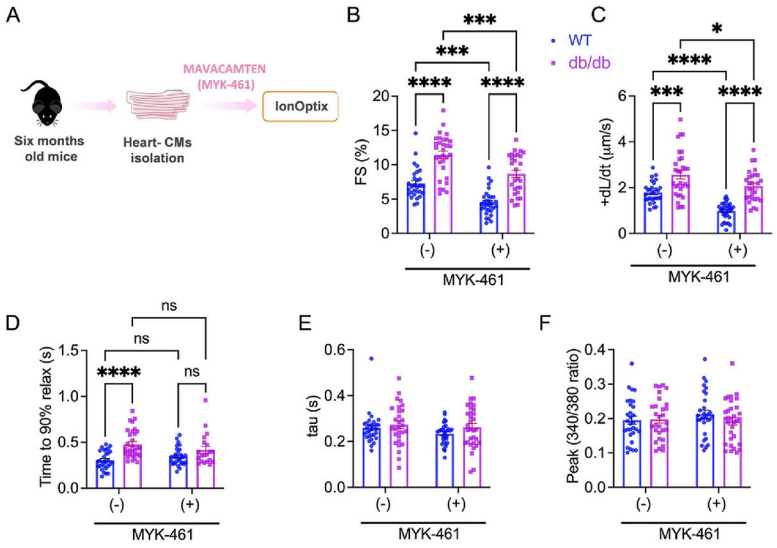

Fig. 5.

Mavacamten improves contractility in isolated cardiomyocytes *in vitro*. As a proof-of-concept, we used freshly isolated cardiomyocytes from wild-type (WT) and *db/db* mice (6 months of age, mixed sex) and measured contractility in the presence of mavacamten (MYK-461) at a concentration of 250 nM (A). Fractional shortening (FS%, B), contraction velocity (C), and time to 90 % relaxation (D) were significantly increased in *db/db* isolated cardiomyocytes, but significantly decreased in cardiomyocytes of *db/db* mice, compared to untreated and control groups, after administration of MYK-461. (E) Relaxation time constant (t) of calcium transient and (F) Calcium amplitude indicated by peak (340/380) in the absence and presence of MYK-461 were not different between the groups. Two-way ANOVA followed by Tukey's *post hoc* test was used; data points were pooled from three independent experiments. Data are expressed as mean ± SE, n = 29 myocytes/3 mice/group. *P ≤ 0.05, ***P ≤ 0.001 and ****P ≤ 0.0001 *db/db vs.* WT.

Table 1

Echocardiographic features in mixed-gender WT and *db/db* mice at six months of age.

Measurements (units)	WT	Lepr^ *db/db*	p-Value
LVEF (%)	53.27 ± 1.526	65.61 ± 1.520	<0.0001
FS (%)	27.09 ± 0.966	35.44 ± 1.190	<0.0001
LV Mass (mg)	71.02 ± 5.741	88.50 ± 3.154	0.0159
LVPW;d (mm)	0.655 ± 0.03	0.804 ± 0.035	0.0421
LVPW;s (mm)	0.975 ± 0.076	1.219 ± 0.055	0.0140
IVS;d (mm)	0.646 ± 0.031	0.941 ± 0.035	<0.0001
IVS; s (mm)	0.721 ± 0.047	1.028 ± 0.044	0.0007
E/A	1.867 ± 0.146	1.511 ± 0.051	0.0144
E/E′	−27.62 ± 1.951	−36.03 ± 2.666	0.0191

All values are expressed as mean ± SEM with the number of mice listed in parentheses beside groups. (*N* = 7–9 mice in each group).

Table 2

F_{max}, pCa_{50}, and k_{tr} for an equal number of papillary fibers of both WT and *db/db* mice treated with and without MYK-461.

Animal	Dose	F_{max} mN/mm^2	pCa_{50}	k_{tr} (s^{-1})
WT	Control	31.9 ± 2.75	5.61 ± 0.02	5.25 ± 1
	2 μM MYK-461	24.9 ± 2.64 **	5.58 ± 0.02	3.32 ± 0.47 **
db/db	Control	42.1 ± 4.72 ¶¶¶¶	5.68 ± 0.03 ¶¶¶	8.84 ± 2.02 ¶¶¶
	2 μM MYK-461	33.8 ± 3.14 §§§	5.61 ± 0.02 §§§	4.332 ± 1.55 §§§§

* $p < 0.05$.

** $p < 0.01$,

*** $p < 0.001$,

**** $p < 0.0001$ WT baseline *versus* WT with MYK-461.

§ $p < 0.05$,

§§ $p < 0.01$,

§§§ $p < 0.001$,

§§§§ $p < 0.0001$ *db/db* baseline *versus db/db* with MYK-461.

¶ $p < 0.05$,

¶¶ $p < 0.01$,

¶¶¶ $p < 0.001$,

¶¶¶¶ $p < 0.0001$ WT baseline *versus db/db* baseline.

Table 3

Contractility and calcium transients parameters for both WT and *db/db* mice treated with and without MYK-461.

	WT		***db/db***	
	(−) MYK461	**(+) MYK461**	**(−) MYK461**	**(+) MYK461**
Contractility measurements				
Fractional shortening (FS%)	7.26 ± 0.41	4.51 ± 0.32	11.43 ± 0.55	8.67 ± 0.54
+dL/dt (μm/s)	1.78 ± 0.08	0.98 ± 0.06	2.56 ± 0.18	2.06 ± 0.12
−dL/dt (μm/s)	0.93 ± 0.11	0.88 ± 0.11	1.10 ± 0.09	1.38 ± 0.16
T50% relax (s)	0.32 ± 0.02	0.29 ± 0.01	0.29 ± 0.01	0.28 ± 0.01
T90% relax (s)	0.30 ± 0.01	0.34 ± 0.01	0.48 ± 0.02	0.42 ± 0.03
Calcium measurements				
Diastolic Ca^{2}+ (340:380)	1.10 ± 0.01	1.12 ± 0.01	1.06 ± 0.06	1.07 ± 0.01
Peak (340:380)	0.19 ± 0.01	0.21 ± 0.01	0.20 ± 0.01	0.19 ± 0.01
Tau (s)	0.26 ± 0.01	0.23 ± 0.01	0.27 ± 0.01	0.26 ± 0.02
T50% Decay (s)	0.25 ± 0.01	0.22 ± 0.02	0.28 ± 0.01	0.28 ± 0.01
T90% Decay (s)	0.65 ± 0.03	0.57 ± 0.03	0.72 ± 0.05	0.68 ± 0.03